Processivity, substrate positioning and binding; the role of polar residues in a family 18 glycoside hydrolase

Anne Grethe Hamre[†1], Suvamay Jana[*1], Nicole K. Reppert[†], Christina M. Payne[*2], and Morten Sørlie[†2]

[†]Department of Chemistry, Biotechnology and Food Science, Norwegian University of Life Sciences, PO 5003, N-1432 Ås, Norway.

[*]Department of Chemical and Materials Engineering, University of Kentucky, Lexington, Kentucky 40506, United States

#Running title: Strong binding polar residues are important for processivity

[1]A. G. Hamre and S. Jana contributed equally to this work.

[2]To whom correspondence should be addressed: E-mail address: morten.sorlie@nmbu.no and christy.payne@uky.edu. Tel.: +47-67232562 and Fax: +47-64965901 (MS); Tel.: + 859-257-2902 and Fax: + 859-323-1929 (CMP).

Keywords: Chitin, cellulose, glycoside hydrolase, chitinase, cellulase, processivity, binding free energy, molecular dynamics

Background: The role of polar residues in mediating processive hydrolysis of recalcitrant polysaccharides is poorly understood.

Results: Polar residues play important roles in processivity and positioning of the substrate.

Conclusion: Beyond the canonical carbohydrate-aromatic stacking interactions, strong binding polar residues can play a key role in processivity

Significance: Complements the understanding of how glycoside hydrolases are able to depolymerize recalcitrant polysaccharides.

ABSTRACT
The enzymatic degradation of recalcitrant polysaccharides such as cellulose (β-1,4-linked glucose) and chitin (β-1,4-linked N-acetylglucosamine) by glycoside hydrolases (GHs) is of significant biological and economical importance. In nature, depolymerization is primarily accomplished by processive GHs, which remain attached to the substrate in between subsequent hydrolytic reactions. Recent computational efforts have suggested that the processive ability of a GH is directly linked to ligand binding free energy. The contribution of individual aromatic residues in the active site of these enzymes has been extensively studied. In the present study, we offer the first experimental evidence confirming correlation of binding free energy and degree of processivity and that polar residues are essential for maintaining processive ability. Exchanging Thr[276] with Ala in substrate binding subsite −2 in the processive ChiA of *Serratia marcescens* results in a reduction of both enthalpy (2.6 and 3.8 kcal/mol) and free

1

energy (0.5 kcal/mol and 2.2 kcal/mol) for the binding to the substrate (GlcNAc)$_6$ and the inhibitor allosamidin, respectively, compared to that of the wild type. Moreover, initial apparent processivity as measured by [(GlcNAc)$_2$]/[GlcNAc] ratios (17.1 ± 0.4 vs. 30.1 ± 1.5) and chitin degradation efficiency (20 % vs. 75 %) are greatly reduced for ChiA-T276A vs. the wild type. Mutation of Arg^{172} to Ala, reduces the recognition and positioning of the substrate into the active site. Molecular dynamics simulations indicate ChiA-R172A behaves similarly to the wild type, but dynamics of ChiA-T276A are greatly influenced by mutation, which is reflective of their influence on processivity.

Chitin and cellulose are insoluble, linear homopolymers consisting of β-1,4 linked *N*-acetyl-glucosamine (GlcNAc; **A**-unit) and β-1,4 linked glucose units, respectively. The individual sugar moieties are rotated 180° relative to each other, yielding a disaccharide structural unit (1). Depolymerization of chitin and cellulose to soluble, dimeric units is typically accomplished through the action of glycoside hydrolases (GHs) known as cellulases and chitinases, respectively. Chitin and cellulose polysaccharides are the two most abundant biopolymers in nature with an annual production amounting to 100 billion and one trillion tons, respectively (2,3). With such massive availability, these polysaccharides represent a nearly unlimited source of raw material for the production of fuels and specialty chemicals through enzymatic approaches. However, efficient enzymatic degradation of these materials is critical to the economic viability of any commercial conversion process. Accordingly, engineering enzymes for new and more efficient conversion requires development of fundamental knowledge of both catalytic mechanisms and the means by which the enzyme interacts with the polysaccharide substrate.

Glycoside hydrolases catalyze the hydrolysis of *O*-glycosidic bonds between two or more carbohydrates or between a carbohydrate and a non-carbohydrate moiety (www.cazy.org (4)). In general, hydrolysis occurs via acid catalysis that requires two critical residues: one proton donor and a nucleophile/base (5). Each enzyme has a

customized mode of action, either by random cleavage of polymer chains (endo-acting enzymes) or by preferential cleavage of the reducing or non-reducing ends of chains (exo-acting enzymes). Both endo- and exo- mechanisms can be combined with processive action, meaning that the enzymes bind individual polymer chains in long tunnels or deep clefts and hydrolyze a series of glycosidic linkages along the same chain before dissociation (6). This range of potential functions has historically made characterization of these enzymes, particularly cellulases, quite difficult.

In nature, processive GHs are the primary enzymes responsible for polysaccharide depolymerization. It is thought that processivity enhances catalytic efficiency by keeping the enzyme closely associated to the substrate in between subsequent hydrolytic reactions and keeping once-detached single chains from re-associating with the insoluble material (7,8). Hydrolysis of recalcitrant polysaccharides by exo-processive enzymes can be divided into at least 4 putative steps: (i) binding to the polymer surface; (ii) recognition and capture of the chain end; (iii) formation of the productive complex and processive hydrolysis of the polymer chain, and; (iv) dissociation (9). For processes ii) and iii), it is vital that individual binding subsites recognize and orient their specific substrates through formation of intermolecular bonds. In protein-carbohydrate complexes, the dominant interactions are hydrogen bonding and carbohydrate-aromatic stacking interactions, which also happen to be the primary determinants of ligand binding free energy. Accordingly, it has been hypothesized that ligand binding free energy may be directly correlated with processive ability. Using free energy calculations, Payne et al. qualitatively illustrated this relationship for Family 7 GHs (10); though, this study was inherently limited given the dearth of experimental measurements of processivity and binding free energy. Experiments quantifying the relationship of binding free energy with processivity do not yet exist.

Stacking or hydrophobic interactions can be formed between aromatic residues, in particular tryptophans, at the binding site of the enzyme and one or both sides of the sugar ring (11,12). Such interactions have been explored in many studies showing that many processive GHs have a path of

conserved solvent exposed aromatic residues leading into the active site cleft (13,14). The hydrophobic interactions create a flexible sheath allowing the polymeric substrate to slide through the active site as well as playing a central role in the binding and guidance of the insoluble substrate into the active site cleft (14-16). Mutagenesis of these aromatic residues nearly abolishes processivity (17-19). Hydrogen bonding can occur between polar residues and sugar-hydroxyl groups that have the potential to be involved in as many as three hydrogen bonds; one as a donor and two as an acceptor (12). Proctor *et al*. showed that the removal of the steric block mediated by the side chains of the polar Gln-316 and Asp-53 at the −3 subsite of the exo-active *Cj*Arb43A from *Cellvibrio japonicus* changed the mode of action to (20). A computational study of a processive *Trichoderma reesei* cellulase implicates polar residues in product inhibition, having the effect of reduced overall turnover (21). Moreover, in a maltooligosaccharide – maltoporin model, it has been shown that the combination of hydrogen bonding and hydrophobic interactions makes a smoother energy profile with regard to processivity than the two interactions alone (22). The latter study highlights the importance of both polar-mediated hydrogen bonding and aromatic-mediated hydrophobic stacking. Nevertheless, the role of polar residues in mediating GH processivity is poorly understood.

The chitinolytic machinery of the gram-negative soil bacteria *Serratia marcescens* offers several advantages toward the study of processive GH action, and thus, is often used as model system for enzymatic degradation of recalcitrant polysaccharides (23-26). The suite of *S. marcescens* chitinases includes two processive enzymes, one of which is chitinase A (ChiA), a Family 18 GH that preferentially acts from the reducing end of the sugar chain. The active site of ChiA has a deep, cleft-like architecture, where the catalytic domain contains 4 substrate (−4 to −1) and 3 product (+1 to +3) binding subsites. The carbohydrate binding module, fused with the catalytic domain, exhibits additional substrate binding sites extending toward the catalytic domain (19,27-29). In the catalytic domain of ChiA, the roles of three aromatic residues (Trp[167], Trp[275], and Phe[396]) in substrate binding,

processivity, and activity have been characterized. Of the three, Trp[167], situated in the −3 substrate binding subsite, was shown to be most important to processivity, efficiency of chitin degradation, and for the recognition and positioning of the substrate before hydrolysis (19,30). A comparable study of the ChiA polar residues will provide a more complete description of the protein-carbohydrate interactions governing processive ability, and further, can shed light on the relationship of binding free energy with processive ability.

In the present study, we investigate the role of two polar residues, Arg[172] and Thr[276], in catalysis of glycosidic linkages, substrate binding, and processivity. These two polar residues have been selected on the basis of their position in the active site, avoiding residues that will clearly abolish activity (as part of the reaction mechanism). Available crystal structures suggest Arg[172] and Thr[276] participate in hydrogen bonding with the substrate, and as such, may play key roles. We apply experimental and computational approaches to uncover the roles of these specific residues. Further, our investigation yields the experimental evidence toward validation of the relationship of binding free energy with processivity. Site directed mutagenesis has been used to obtain R172A and T276A variants. We have characterized the effects of these mutations with respect to wild-type using standard enzymological methods to determine apparent processivity (HPLC), the equilibrium binding association constant (K_a) and $\Delta H°_r$ (isothermal titration calorimetry (ITC)), and the preference of acetylated and deacetylated units in the different subsites (mass spectrometry (MS)). To understand the molecular-scale effects these residues have on substrate binding, molecular dynamics simulations of the wild-type and variants have been conducted.

EXPERIMENTAL PROCEDURES

Chemicals.

Chito-oligosaccharides (CHOS) were obtained from Megazyme (Wicklow, Ireland). Squid pen *β*-chitin was purchased from France Chitin (180μm microparticulate, Marseille, France). Allosamidin was isolated from *Streptomyces sp.,* and the purity was controlled by ^{1}H NMR as described elsewhere (31). Previously, the structure of allosamidin has

3

been verified by both NMR and crystallography (32). All other chemicals were of analytical grade.

Enzymes.

Site directed mutagenesis

Mutagenesis of ChiA-R172A, ChiA-T276A, ChiA-E315Q-R172A, and ChiA-E315Q-T276A was performed using the QuikChange™ site directed mutagenesis kit from Stratagene (La Jolla, CA, USA), as described by the manufacturer. To concentrate the DNA, the Pellet Paint® Co-precipitant kit from Novagen (Madison, WI, USA) was used as described in the product manual. The primers and templates used for the mutagenesis are listed in Table 1 and were purchased from Life Technologies (Carlsbad, CA, USA). To confirm that the genes contained the desired mutations and to check for the occurrence of nondesirable mutations, the mutated genes were sequenced using GATC Biotech's (Constance, Germany) LIGHTrun Sequencing service before they were transformed into *Escherichia coli* BL21Star (DE3) cells (Life Technologies, Carlsbad, CA, USA).

Construction of His$_{10}$-ChiA-E315Q-R172A and His$_{10}$-ChiA-E315Q-T276A

In order to subclone the inactive mutants ChiA-E315Q-R172A and ChiA-E315Q-T276A from pMay2-10 to pET16b (Novagen, Madison, WI, USA), the chitinase fragments were amplified by PCR to introduce NdeI and XhoI restriction sites. PCR reactions were conducted with Q5® High-fidelity 2X Master Mix (New England Biolabs, Ipswich, MA). The amplification protocol consisted of an initial denaturation cycle of 30 s at 98 °C, followed by 30 cycles of 5 s at 98 °C, 30 s at 55 °C, 30 s at 72 °C, and a final step of 2 min at 72 °C. The following primers, purchased from Life Technologies (Carlsbad, CA, USA), were used in the PCR reaction: 5'TCGAAGGTCGTCATATGGCCGCGCCGGG C'3 (forward) and 5'CAGCCGGATCCTCGAGTTATTGAACGCC GGCGC'3 (reverse). The amplified insert was subcloned via NdeI and XhoI (New England Biolabs, Ipswich, MA, USA) restriction sites into pET16b by using the In-Fusion HD Cloning kit (Clontech Laboratories, Kyoto, Japan). The resulting pET16b constructs were sequenced using GATC Biotech's (Constance, Germany) LIGHTrun sequencing service to confirm the correct insert before they were transformed into *E. coli* Rosetta 2(DE3) cells (Life Technologies, Carlsbad, CA, USA).

Protein expression and purification of single mutants

ChiA-R172A and ChiA-T276A genes were expressed in *E. coli* as described previously (33,34). For protein purification, the periplasmic extracts were loaded on a column packed with chitin beads (New England Biolabs) (1.5 cm in diameter, 10 ml stationary phase in total) and equilibrated in 50 mM Tris-HCl pH 8.0. After washing the column with the same buffer, the enzymes were eluted with 20 mM acetic acid. The buffer was then changed to 100 mM Tris-HCl (pH 8.0) using Macrosep Advance Centrifugal Device (30 kDa cutoff, Pall corporation, Port Washington, USA). Enzyme purity was verified by SDS-PAGE, and protein concentrations were determined by using the Bradford protein assay from Bio-Rad (Hercules, CA, USA).

Protein expression and purification of double, inactive mutants

For protein expression, *E. coli* Rosetta 2(DE3) cells containing the appropriate plasmid (ChiA-E315Q-R172A, ChiA-E315Q-T276A) were inoculated into 25 mL Terrific Broth (TB) medium containing 115 µg/mL ampicillin and 50 µg/mL chloramphenicol and grown at 37 °C and 200 rpm for 16 h. Cell culture were then inoculated into 250 mL TB medium containing 115 µg/mL ampicillin and 50 µg/mL chloramphenicol to an OD$_{600}$ of 0.1. This culture was cultivated until the OD$_{600}$ reached 0.8-1.0. The temperature was decreased to 22°C, and gene expression was induced with 1 mM isopropyl-β-D-thiogalactopyranoside for 20 h. The cells were harvested by centrifugation (8000 rpm, 20 min at 4 °C). Periplasmic fractions were prepared by osmotic shocking as described elsewhere (35). A cytoplasmic protein extraction was also performed by re-suspending the spheroplasts in lysis buffer (0.1 mg/mL lysozyme, 50 mM Tris-HCl, 50 mM NaCl, 4 mM MgCl$_2$, 1 mM EDTA, 0.1 mM PMSF; pH 8.0) before incubating it at 37 °C for 30 min. Cell debris was removed by centrifugation (8000 rpm, 20 min at 4 °C). The resulting supernatant was used for further enzyme purification. Both the periplasmic and

4

cytoplasmic extracts were sterilized by filtration (0.2 µm) prior to protein purification.

Proteins were purified on a column packed with Ni-NTA Agarose matrix (Qiagen, Venlo, Netherlands) (1.5 cm in diameter, 5 ml stationary phase in total). The column was pre-equilibrated in buffer A (20 mM Tris-HCl, 20 mM imidazole, 500 mM NaCl, pH 8.0) before the periplasmic and cytoplasmic extracts were applied. After washing with buffer B (20 mM Tris-HCl, 500 mM NaCl, pH 8.0), fractions containing the enzyme were eluted with buffer C (20 mM Tris-HCl, 250 mM imidazole, 500 mM NaCl, pH 8.0). A flow rate of 2.5 mL/min was used at all times. Enzyme purity was verified by SDS-PAGE, and fractions containing purified enzyme were concentrated and transferred (Macrosep Advance Centrifugal Device, 30 kDa cutoff, Pall corporation, Port Washington, USA) to 20 mM potassium phosphate buffer pH 6.0. Enzyme purity was verified by SDS-PAGE while protein concentrations were determined by using the Bradford protein assay from Bio-Rad (Hercules, CA, USA).

Degradation of chitosan

Chitosan was dissolved in 80 mM sodium acetate buffer (pH 5.5) to a final concentration of 10 mg/mL as described previously (36). Chitosan with a fraction of *N*-acetylated units (F_A) = 0.65 was depolymerized by adding 2.5 µg enzyme per 1 mg chitosan. The reactions were run to completion (maximum degree of scission (α)) before enzyme activity was stopped by lowering the pH with 150 µL 1 M HCl and 2 minutes boiling (36).

2-aminoacridone derivatization and sequence determination of chito-oligosaccharides

In order to determine the sequence of chitosan oligomers, the oligosaccharides were derivatized by reductive amination of the reducing end with 2-aminoacridone (AMAC) as described previously (37,38).

Matrix assisted laser desorption/ionization mass spectrometry

Sequencing of the pentameric chitosan oligomers (degree of polymerization (DP) = 5) was performed using matrix assisted laser desorption/ionization time-of-flight/time-of-flight mass spectrometry/mass spectrometry (MALDI-TOF/TOF-MS/MS) as described earlier (37). MS

spectra were acquired using an UltraflexTM TOF/TOF mass spectrometer (Bruker Daltonik GmbH, Bremen, Germany) with gridless ion optics under control of Flexcontrol. For sample preparation, 1 µl of the reaction products was mixed with 1 µl 10 % 2,5-dihydroxybenzoic acid (DHB) in 30 % ethanol and spotted onto a MALDI target plate. The MS experiments were conducted using an accelerating potential of 20 kV in the reflectron mode.

Degradation of chitin

Hydrolysis of chitin was carried out as described previously (39). The extent of degradation is defined as the percentage of number of moles of solubilized GlcNAc-units with respect to number of moles GlcNAc-units in solid form (chitin) used in the experiments.

High performance liquid chromatography (HPLC)

Concentrations of mono- and disaccharides were determined using HPLC with a Rezex Fast fruit H$^+$ column (100 mm length and 7.8 mm inner diameter) (Phenomenex). An 8 µl sample was injected on the column, and the mono- and disaccharides were eluted isocratically at 1 mL/min with 5 mM H_2SO_4 at 85 °C. The mono- and disaccharides were monitored by measuring absorbance at 210 nm, and the amounts were quantified by measuring peak areas. Peak areas were compared with peak areas obtained with standard samples with known concentrations of mono- and disaccharides.

Isothermal Titration Calorimetry

ITC experiments were performed with a VP-ITC system from Microcal, Inc. (Northampton, MA) (40). Solutions were thoroughly degassed by vacuum pump prior to experiments to avoid air bubbles in the calorimeter. Standard ITC conditions were 250 µM of allosamidin or 500 µM of hexa-*N*-acetyl glucosamine (GlcNAc)$_6$ in the syringe and 15 µM of enzyme in the reaction cell in 20 mM potassium phosphate buffer of pH 6.0. The only exception was for ChiA-E315Q-T276A against (GlcNAc)$_6$. To ensure a *c*-value between 10 and 1000, which is a prerequisite for meaningful calculations of K_a (40), 1 mM (GlcNAc)$_6$ and 30 µM enzyme were used yielding a *c*-value of 25. Aliquots of 4-8 µl were injected into the reaction cell at 180s intervals at 30 °C with a stirring speed

of 260 rpm. 45 injections were performed. At least three independent titrations were performed for each binding reaction.

Analysis of calorimetric data

ITC data were collected automatically using the Microcal Origin v.7.0 software accompanying the VP-ITC system (40). Prior to further analysis, data were corrected for heat dilution by subtracting the heat remaining after saturation of binding sites on the enzyme. Data were fitted using a non-linear least-squares algorithm using a single-site binding model employed by the Origin software that accompanies the VP-ITC system. All data from the binding reactions fit well with the single site binding model yielding the stoichiometry (n), equilibrium binding association constant (K_a), and the reaction enthalpy change ($\Delta H_r°$) of the reaction. The equilibrium binding dissociation constant (K_d), reaction free energy change ($\Delta G_r°$) and the reaction entropy change ($\Delta S_r°$) were calculated from the relation described in Equation 1.

$$\Delta G_r° = -RT\ln K_a = RT\ln K_d = \Delta H_r° - T\Delta S_r° \qquad (1)$$

Errors are reported as standard deviations of at least three experiments.

Kinetic Analysis

The kinetic constants, k_{cat} and K_m, of the ChiA-T276A and ChiA-R172A mutants were determined using $(GlcNAc)_4$ substrate (41,42), which at the substrate concentrations and in the time frames used for kinetic analysis, is hydrolyzed into two dimers by both enzyme variants in this study. Reaction mixtures, with 10 different $(GlcNAc)_4$ concentrations varying from 2 to 100 μM in 20 mM sodium acetate buffer, pH 6.1 and 0.1 mg/mL BSA (final concentrations), were pre-incubated in a 37 °C water bath for 10 min prior to starting the reactions. The reactions were started by adding purified enzyme to reach an enzyme concentration of 0.2 nM (ChiA-R172A) and 1 nM (ChiA-T276A) in a total reaction volume of 1.0 mL. To determine the rate of $(GlcNAc)_4$ hydrolysis at a specific concentration, seven 75-μL samples, including one at time equal zero, were withdrawn at regular time intervals over a total period of 1 − 10 min, and the enzyme was inactivated by adding 75 μL of 20 mM H_2SO_4. All of the reactions were run in duplicate, and all of the samples were stored at −20 °C until HPLC analysis. Reaction

conditions were such that the rate of hydrolysis of $(GlcNAc)_4$ was essentially constant over time, with the $(GlcNAc)_4$ concentration always staying above 80% of the starting concentration. Data points were only discarded when hydrolysis had not taken place or more than 20% of the initial $(GlcNAc)_4$ were hydrolyzed (to ensure initial rates only). If more than two of the seven data points had to be removed due to the reasons described above, the whole set was discarded. The slopes of plots of 0.5 times the $(GlcNAc)_2$ concentration versus time were taken as the hydrolysis rate. The rates were plotted versus substrate concentration in a Michaelis−Menten plot, and the experimental data were fitted to the Michaelis−Menten equation by nonlinear regression using Origin v7.0 (OriginLab Corp., Northampton, MA).

Molecular dynamics (MD) simulations

Classical MD simulations were constructed for the three ChiA systems: ChiA-WT, ChiA-R172A, and ChiA-T276A. The initial coordinates for all three MD simulation sets were from the protein data bank entry 1EHN (27). The E315Q mutation of the 1EHN structure was reversed in each case using the PyMOL mutagenesis tool. Similarly, the R172A and T276A variants were constructed from the wild-type coordinates. The $(GlcNAc)_6$ ligand was also obtained from 1EHN. The deposited structure exhibits a $(GlcNAc)_8$ ligand bound from the −6 to +2 binding subsites. In accordance with experimental protocol, we manually shortened this ligand by deleting the atoms in the −6 and −5 subsites, leaving a bound $(GlcNAc)_6$ in the −4 to +2 sites. The acetyl group of the −1 pyranose ring and the side chain of Asp[313] were manually rotated around their range of dihedrals, such that the catalytic residues and the −1 sugar reflected the catalytically active conformation of a Family 18 chitinase (43). The protonation states for each simulation were determined using H++ at a pH of 6.0 and an internal and external dielectric constant of 10 and 80, respectively (44-46). Two disulfide bridges observed in the structure also covalently bonded, between Cys[115] and Cys[120] and Cys[195] and Cys[218]. Sodium ions were added to each system to ensure the total system charge equaled zero.

The constructed systems were then minimized in vacuum, solvated, and re-minimized. The vacuum minimizations were performed to remove any

6

initial bad contacts between overlapping atoms as a result of the addition of hydrogens. The initial minimization protocol included 1000 iterations of steepest descent (SD) followed by 1000 iterations of adopted basis Newton Raphson (ABNR), each applied to the entire protein-ligand complex. The minimized systems were then solvated in explicit TIP3P water. The periodic boundary conditions were 120 Å x 120 Å x 120 Å. This box size was selected such that the protein had a minimum of 10 Å solvent buffer on each side. The total system size for each simulation is approximately 175,000 atoms. The solvated systems were then minimized again according to a stepwise protocol: (1) the water molecules were minimized for 10,000 SD steps, keeping the protein and ligand rigid; (2) the protein and water were then minimized for 10,000 SD steps keeping the ligand fixed; and (3) the entire system was minimized for 10,000 steps using SD.

The completely constructed systems were then heated and equilibrated prior to collection of production MD simulation data. In all cases, the CHARMM36 all-atom force field with CMAP (47-49) corrections was used to model the protein and carbohydrate interactions, and water was modeled with the modified TIP3P (50,51) force field. The systems were heated from 100 K to 300 K in 50 K increments over the span of 4 ps. The system density was equilibrated in the NPT ensemble for 100 ps. The Nosè-Hoover thermostat and barostat were used for pressure control (52,53). The systems were constructed, minimized, heated, and equilibrated using CHARMM (47).

After equilibration, the simulations were moved into the NAMD simulation package for efficient integration (54). In the NVT ensemble, 250-ns simulations were performed of each of the three systems at 300 K. The periodic volumes were based on the final values from the NPT equilibrations in CHARMM. Each simulation used a 2-fs time step for the integration scheme. The Particle Mesh Ewald method was used to describe long-range electrostatics with a sixth order b-spline, a Gaussian distribution width of 0.312 Å, and a 1 Å grid spacing (55). A non-bonded cutoff distance of 10 Å, a switching distance of 9 Å, and a non-bonded pair list distance of 12 Å were used. All hydrogen atom distances were fixed using the SHAKE algorithm (56). VMD was used for visualization of all the trajectories and hydrogen bond analysis (57). Hydrogen bond formation was determined using a 3.4 Å distance cutoff along with an angle cutoff of 60°.

Results

Mutant design and initial mutant characterization

ChiA is exo-processive acting from the reducing end of the substrate. According to accepted naming convention, ChiA substrate binding subsites are identified by negative numbers, with hydrolysis occurring between the −1 and +1 binding sites (58). Several important intermolecular interactions between the chito-oligosaccharide substrate and the enzyme occur in substrate binding subsites −2, −3, and −4 (Figure 1), as discussed by Norberg and co-workers (30). Arg^{172} is notable in that it appears to interact with the substrate in three subsites, −2, −3, and −4, rather than through a single proximal interaction. From examination of the crystal structure, Arg^{172} interacts with the acetyl group carbonyl oxygen in the −4 subsite. Though, the −2 subsite GlcNAc is too distant to form an interaction with Arg^{172}, the charged protein side chain is thought to be a part of an electrostatic-dipole interaction with the C3 secondary alcohol or the acetyl group. In subsite −3, Arg^{172} appears to participate in a bifurcated hydrogen bond to the GlcNAc primary alcohol, in conjunction with Glu^{473}.

Similarly, the crystal structure indicates Thr^{276} interacts with both the −2 and −3 GlcNAc moieties. In the −3 subsite, the threonine OH group forms a hydrogen bond with the substrate carbonyl oxygen. Thr^{276}, together with Trp^{275}, forms hydrogen bonds with the −2 GlcNAc primary alcohol through the protein backbone. Given the ability of Arg^{172} and Thr^{276} to form strong electrostatic − dipole interactions and their proximity to multiple hydrogen bonding partners along the length of the active site cleft, we anticipate each residue plays a role in substrate binding, processivity, and possibly catalytic turnover. Mutating these residues to alanine effectively abolishes the electrostatic potential of the residue and negates the ability to hydrogen bond except through backbone-mediated interactions. This latter point is particularly important for examination of the effect of mutating Thr^{276} to alanine, where loss in binding or

processive ability may then be attributed to interaction of Thr[276] with the carbonyl oxygen in the −3 subsite.

To initially assess activity of the constructed mutants, k_{cat} and K_m were determined using the natural substrate (GlcNAc)$_4$, which has been shown to be the best soluble substrate to obtain Michaelis-Menten kinetics for family 18 chitinases (41). Moreover, previous work has shown that effects of mutations in the −2 and −3 subsites manifest in the kinetics of (GlcNAc)$_4$ hydrolysis (30,42). In the substrate concentration range studied, both mutants showed straightforward Michaelis-Menten kinetics without substrate inhibition, as also previously shown for ChiA-WT. The kinetic parameters are listed in Table 2.

Degradation of chitosan

Deacetylation of chitin yields the water-soluble, heterologous de-*N*-acetylated analog, chitosan, that consists of linear β-1,4-linked *N*-glucosamine (GlcN; **D**-unit) and GlcNAc units (59,60). It can be prepared with varying amount and pattern of *N*-acetylated units as well as varying length of the polymer chain (61,62). Characteristic of Family 18 GHs, chitinases degrade chitin with retention of the stereochemistry at the anomeric carbon (www.cazy.org (4)). They also employ a specialized substrate-assisted mechanism in which the *N*-acetyl group of the sugar in subsite −1 acts as the nucleophile (43,63-65). As a result, Family 18 chitinases have an absolute preference for acetylated units in this subsite. For this reason, degradation of chitosan by chitinases has proven to be a useful tool in the determination of both processivity (19,36) as well as substrate positioning (30). In this study, chitosan with a degree of acetylation of 65 % was degraded by ChiA-R172A and ChiA-T276A to a maximum degree of scission. The pentameric products obtained were labeled at the reducing end and analyzed with respect to sequence of acetylated and deacetylated units by reducing end labeling and MALDI-TOF-TOF-MS/MS (38). Such sequences detail the preferences each individual subsite has for acetylated vs. deacetylated units, and hence, show its importance in recognizing and positioning of the substrate before hydrolysis (30,37). Beyond the absolute preference for an **A** in subsite −1 for each enzyme, the sequences

(Table 3) illustrate a preference for an acetylated unit in subsites −3 and −4 for ChiA-T276A while ChiA-R172A has no strong preferences as seen by the many different sequences present. In comparison, ChiA-WT has a preference for an acetylated unit in subsites −1, −2, and −4 (30).

Degradation of chitin

Apparent processivity (P^{app}) is defined as the average number of consecutive catalytic cycles performed per initiated processive run (either through endo- or exo-mode of attachment) along the crystalline substrate. This value can be measured by a number of different methods, depending on the substrate (39,66,67). A common means of measuring P^{app} in chitinases is by determining the [(GlcNAc)$_2$/(GlcNAc)] ratio. Given the requirement for the *N*-acetyl group in hydrolysis, this approach yields consistent results in determining processive degradation of chitin polysaccharides. In the case of a processive enzyme, the first cleavage from a polymer chain end will result in the release of an odd-numbered oligosaccharide (e.g., mono- or trisaccharide), whereas all subsequent cleavages result in the production of disaccharides because of the 180° rotation of the GlcNAc-units. For non-processive enzymes, the same measurement will result in a random distribution of oligosaccharide lengths. In each case, the steady-state ratio of dimers to monomers represents the relative processive ability; neither processive nor non-processive chitinases are capable of hydrolyzing (GlcNAc)$_2$. Lower ratios are indicative of more initiated runs associated with the inability to maintain prolonged substrate association. The [(GlcNAc)$_2$/(GlcNAc)] ratio is valid if it is assumed that the first product is a trisaccharide that subsequently is hydrolyzed to a mono- and disaccharide (39,66).

P^{app} tends to decrease as the substrate is consumed, most likely because the substrate becomes enriched with recalcitrant regions where there are fewer obstacle-free paths for processive enzyme attachment (39,67,68). Without the addition of accessory enzymes and glucosidases, the enzymes eventually encounter obstacles or fail to release from the substrate causing traffic jams of unproductively bound enzymes. It is thus important to assess processivity during the early stages of the reaction (39). Here, initial

degradation of β-chitin yielded [(GlcNAc)$_2$/(GlcNAc)] ratios of 25.9 ± 0.9 and 17.1 ± 0.4 for ChiA-R172A and ChiA-T276A, respectively. The value for ChiA-WT has previously been determined to be 30.1 ± 1.5 (Figure 2) (39). Furthermore, earlier studies demonstrate a positive correlation between processive ability and rate of GH-catalyzed polysaccharide hydrolysis (25,39,67,69). By examining initial rates of chitin degradation as determined by product formation vs. time (Figure 3), it is clear that ChiA-WT, the most processive, is faster than ChiA-T276A, the least processive, with ChiA-R172A being intermediate.

Finally, distinct differences between the three enzymes can also be seen with regard to the degradation efficiency. ChiA-WT has the ability to degrade 75 % of the β-chitin while 50 % is degraded by ChiA-R172A. Only 20 % β-chitin is degraded when ChiA-T276A is used (Figure 4).

Thermodynamics

To assess the contribution Arg^{172} and Thr^{276} have on the binding free energy between ChiA and substrate, ITC measurements were taken for the individual mutants binding the soluble substrate (GlcNAc)$_6$ and the well-known inhibitor allosamidin. Both ligands are similar to the natural substrate and span the important catalytic subsites −3 to −1 (Figure 1). When allosamidin is the ligand, catalytically active enzymes can be applied (less perturbation of the system), in contrast to when (GlcNAc)$_6$ is the ligand and catalytically inactivated enzymes (mutation of the catalytic Glu to Gln) must be used.

The binding of (GlcNAc)$_6$ to ChiA-WT was undertaken at pH 6.0 (20 mM potassium phosphate buffer) and 30 °C. To determine the (GlcNAc)$_6$ binding thermodynamics, an inactive variant of the enzyme was used. Thus, the free energy values of (GlcNAc)$_6$ were determined with a single point mutation (E315Q) representing wild-type and double mutations for ChiA-R172A and ChiA-T276A. A typical thermogram and theoretical fit to the experimental data is given in Figure 5. ChiA binds (GlcNAc)$_6$ with a K_d of 0.56 ± 0.03 μM, corresponding to a free energy change ($\Delta G_r°$) of −8.7 ± 0.1 kcal/mol, an enthalpic change ($\Delta H_r°$) of −4.5 ± 0.2 kcal/mol, and an entropic change ($\Delta S_r°$) of 13.9 ± 0.7 cal/K mol ($-T\Delta S_r° = -4.2 \pm 0.2$

kcal/mol) (Table 4). The K_d for the binding between ChiA-R172A and (GlcNAc)$_6$ equals 0.61 ± 0.02 μM with a $\Delta G_r° = -8.6 \pm 0.1$ kcal/mol, Table 4). The reaction is accompanied by a $\Delta H_r° = -4.8 \pm 0.2$ kcal/mol and a $\Delta S_r° = 12.5 \pm 0.7$ cal/K mol ($-T\Delta S_r° = -3.8 \pm 0.2$ kcal/mol). For ChiA-T276A, the binding has a $K_d = 1.2 \pm 0.2$ μM ($\Delta G_r° = -8.2 \pm 0.1$ kcal/mol) and a $\Delta H_r°$ and $\Delta S_r°$ of −1.9 ± 0.2 kcal/mol and 20.8 ± 0.7 cal/K mol ($-T\Delta S_r° = -6.3 \pm 0.2$ kcal/mol), respectively.

The binding of allosamidin to ChiA-WT has previously been measured at pH 6.0 (20 mM potassium phosphate buffer) and 30 °C using ITC (70) (Table 4). In our study, the binding to ChiA-R172A and ChiA-T276A was studied under the same conditions for direct comparison. Figure 5 shows typical ITC thermograms and theoretical fits to the experimental data for each enzyme. For ChiA-R172A, the binding has a $K_d = 0.067 \pm 0.008$ μM ($\Delta G_r° = -9.9 \pm 0.1$ kcal/mol, Table 4). The reaction is accompanied by a $\Delta H_r°$ of −7.1 ± 0.1 kcal/mol and a $\Delta S_r°$ of 9.2 ± 0.3 cal/K mol ($-T\Delta S_r° = -2.8 \pm 0.1$ kcal/mol). The binding between ChiA-T276A and (GlcNAc)$_6$ has a $K_d = 1.0 \pm 0.1$ μM ($\Delta G_r° = -8.3 \pm 0.1$ kcal/mol) and a $\Delta H_r°$ and $\Delta S_r°$ of −3.7 ± 0.2 kcal/mol and 15.2 ± 0.7 cal/K mol ($-T\Delta S_r° = -4.6 \pm 0.2$ kcal/mol), respectively (Table 4).

Interestingly, the binding affinity of both (GlcNAc)$_6$ and allosamidin to ChiA-WT and ChiA-R172A is virtually identical, while ligand binding affinity to ChiA-T276A is significantly weaker. Moreover, the reduced affinity of (GlcNAc)$_6$ and allosamidin for ChiA-T276A is due to less favorable enthalpy changes (2.6 and 3.8 kcal/mol, respectively), signifying a weaker binding interaction between the protein and the ligand when a threonine is substituted with an alanine.

Molecular Dynamics

Molecular dynamics simulations were performed to obtain molecular-level insight into the experimental observations of binding free energy and apparent processivity measurements. From the 250-ns MD trajectories of ChiA-WT, ChiA-R172A, and ChiA-T276A, we calculated three different quantities related to physical behavior in the active site. First, we calculated the root mean square fluctuation (RMSF) of the hexamer ligand

on a per-binding-site basis (Figure 6A). This value represents the degree to which the ligand fluctuates in its binding site, as referenced against the average structure. Uncertainty was estimated using block averaging; the standard deviation of 2.5 ns blocks of data is shown in the figure. The ligand bound to ChiA-R172A behaves similarly to ChiA-WT. By comparison, the ChiA-T276A ligand fluctuates significantly more than either ChiA-WT or ChiA-R172A along the length of the active site.

In a similar fashion, the RMSF of the catalytic tetrad, Asp[313], Glu[315], Tyr[390], and Asp[391], reveals that the ChiA-T276A catalytic center exhibits a greater degree of freedom (Figure 6B). The tetrad of residues selected are either directly involved in catalysis or are known to play a key role in stabilization of the catalytically active conformation of the ligand, in which the −1 pyranose ring displays a $^{1,4}B$ boat conformation (27). The RMSF value here again represents the average degree of fluctuation of these four residues alone, as compared to the average structure. Block averaging of 2.5 ns data blocks was used to determine uncertainty. The ChiA-R172A catalytic center fluctuates to the same extent as ChiA-WT. As we will discuss below, the prior two simulation observations are thought to be indicative of processive ability or lack thereof (71).

The effect of the R172A and T276A mutations on the conformation of the ligand in the active site was also evaluated. Specifically, we were interested in the effect each mutation had on the ability of the enzyme to maintain the energetically unfavorable skew conformation in the −1 binding site. Ring distortion in the −1 binding site is a notable requirement of glycoside hydrolases, where the catalytic itinerary invariably passes through a skew, boat, envelope, or otherwise distorted conformation to effect catalysis (72,73). ChiA-WT initially exhibits a $^{1,4}B$ conformation in the −1 binding site. Unless catalysis takes place, relieving distortion, the $^{1,4}B$ conformation should be maintained throughout the simulations. Periodic jumps to other conformations can be expected, but prolonged occupation of the relaxed chair conformation is suggestive of a fundamental change in the active site behavior, though not necessarily inactivation. To determine this conformation, we measured the Cremer-Pople ring pucker amplitude, which is a geometric measure of

a ring's conformation, over the course of the 250-ns simulation (Figure 6C) (74). A boat conformation will have an amplitude of 0.73 Å, while a chair conformation will have an amplitude of 0.57 Å (75). Both ChiA-WT and ChiA-R172A maintain the $^{1,4}B$ conformation of the −1 pyranose ring over the entire 250-ns simulation. At approximately 130 ns, the ChiA-T276A ligand relaxes to the chair conformation and never recovers the distortion. The latter behavior suggests that the T276A mutation affords the ligand a lower degree of affinity and more flexibility for relaxation; the length of time required to relax the −1 sugar conformation reflects the distance of the T276A mutation from the catalytic center (−1/+1 binding sites).

Discussion

The possibility that GH binding affinity and degree of processivity is correlated was recently described in a computational study of five processive Family 7 cellulases (10). Using thermodynamics of chemical equilibrium and a previously defined statistical definition of processivity (67), intrinsic processivity (P^{Intr}), Payne *et al.* defined a mathematical relationship between ligand binding free energy and intrinsic processivity (Equation 1),

$$-\Delta G_b°/RT = \ln(P^{Intr} * k_{on}/k_{cat}) \qquad (1)$$

where R is the universal gas constant, T is the temperature, P^{Intr} is intrinsic processivity, k_{on} is the association rate coefficient, and k_{cat} is the catalytic rate coefficient. The relationship in Equation 1 is thought to be general to processive GHs; though, this has not been explicitly demonstrated. Further, the difficulties associated with validating the relationship in cellulases are multitude. Degree of processivity is difficult to accurately quantify, particularly for cellulases, as they do not make use of a substrate-assisted mechanism (66), and the values vary significantly by laboratory. Until recently, the free energy of binding a cello-oligomer to the entire processive cellulase active site had also not been reported (76). Even now, this information is available for only a single *T. reesei* cellobiohydrolase. Accordingly, Payne *et al.* used an enhanced sampling free energy methodology to calculate the binding free energies of five Family 7 GHs. Of these five enzymes, self-consistent processivity measurements were available for two

cellulases, which served as the basis for substantiating a link between calculated binding free energies and processivity (67). Thus far, additional experimental evidence has not been made available by which to quantitatively or qualitatively confirm the relationship in Equation 1.

To describe how our results pertain to Equation 1, we must address the terms 'apparent' and 'intrinsic' processivity. The degree of processivity reported here are measurements of apparent processivity, a value that includes contributions from variables such as substrate heterogeneity and environmental conditions. Intrinsic processivity can be thought of as the theoretical limit of processive ability, under ideal conditions. While Equation 1 was developed with respect to intrinsic processivity, apparent processivity can be used to confirm a qualitative relationship. The experiments performed here have been conducted under the same conditions, and thus, confounding environmental variables will contribute equally to each measurement.

The ligand binding free energies of ChiA-WT, ChiA-R172A, and ChiA-T276A alongside measurements of apparent processivity provide the first complete experimental data set illustrating qualitative agreement with Equation 1. This relationship implies that the stronger an enzyme binds to the substrate, the more processive ability it will have, up to a maximum value, after which the enzyme becomes inhibited by the substrate. We therefore set out to examine the relationship between binding free energy and processivity using a model chitinase system, in which measurements of binding affinity and processivity are more straightforward than for cellulase systems. The mutations R172A and T276A were selected such that the effects of polar residues on binding free energy and processivity could also be assessed. Initial $[(GlcNAc)_2/(GlcNAc)]$ ratios show that exchange of Arg^{172} to Ala only slightly alters the initial degree of processivity (P^{app} of 25.9 ± 0.9 vs. 30.1 ± 1.5). The impact is significantly larger when Thr^{276} is exchanged to Ala with a reduction in P^{app} to 17.1 ± 0.4. The T276A mutation clearly reduces the degree of processivity. As a comparison, the non-processive endo-chitinase ChiC, also from *S. marcescens*, display a P^{app} of 14.3 ± 1.4 (39). The free energy

changes for binding $(GlcNAc)_6$ to ChiA-WT, ChiA-R172A, and ChiA-T276A indeed reveal a correlation between the degree of processivity and binding strength. ChiA-WT and ChiA-R172A bind $(GlcNAc)_6$ with approximately the same affinity, and the processive ability of ChiA-R172A is only moderately lower than the wild-type. The reduced affinity of ChiA-T276A is reflected in its reduced processive ability. This relationship is even clearer in examining the binding affinity of the allosamidin inhibitor to the three enzymes. The slightly reduced affinity of ChiA-R172A for allosamidin, compared to wild-type, reflects the slightly lower processive ability. This phenomenon, inhibitor binding more closely trending with processivity, is likely related to the use of inactive variants in the $(GlcNAc)_6$ ITC measurements. It is suggestive of an experimental design approach, should binding affinity-based predictions of processive ability become a standard tool.

The changes in enthalpic and entropic components of binding free energy resulting from the T276A mutation indicate Thr^{276} plays a significant role in the weak interactions, such as van der Waals interactions and hydrogen bonding, that maintain the rigidity of the bound ligand. The less processive ChiA-T276A exhibits significantly reduced binding free energy change towards both $(GlcNAc)_6$ and allosamidin compared to the wild-type (0.5 kcal/mol and 2.2 kcal/mol, respectively). In general, $\Delta H_r°$ reflect changes in weak interactions (i.e. hydrogen bonds, electrostatic and polar interactions) between the ligand and the enzyme compared to those with the solvent. The differences in $\Delta H_r°$ for $(GlcNAc)_6$ and allosamidin binding to ChiA-T276A vs. the wild type are even more pronounced than the $\Delta G_r°$ values with a decrease of 2.6 and 3.8 kcal/mol respectively. Enthalpy-entropy compensation, where removal of a strong binding interaction may allow for a gain in entropy through more flexibility in the protein-substrate interactions, negates a full conversion of the reduced enthalpy change into free energy change (77).

Molecular dynamics simulations support the observation that the active sites of ChiA-WT and ChiA-R172A behave similarly and that ChiA-T276A is a clear outlier. Four characteristic measurements of active site dynamics were

11

determined from 250-ns MD simulations of the three enzymes: hydrogen bonding patterns, the RMSF of the bound $(GlcNAc)_6$ ligand, the RMSF of the protein catalytic center, and the −1 pyranose ring pucker amplitude. Each of these measurements indirectly reflects binding affinity and was expected to illustrate the above-described trend, namely that enzymes with more flexible/dynamic active sites will have a lower binding affinity and lower processive ability.

As previously mentioned, the ligand-bound ChiA crystal structure depicts an interaction of the Thr[276] OH functional group with the carbonyl oxygen of the −3 pyranose moiety. Along with Trp[275], Thr[276] also mediates hydrogen bonding with the primary alcohol of the -2 site pyranose ring through the backbone (30). Mutating Thr[276] to alanine effectively abolished hydrogen bonding with the −3 sugar (Figure 7A). Backbone mediated hydrogen bonding with the −2 site was still feasible, though slightly reduced in number of hydrogen bonds formed (Figure 7B). The loss of interaction with the −3 site in the T276A ChiA variant greatly affects ligand stability in the −2 to +2 binding sites (Figure 6A). The lost hydrogen bond between the Thr[276] side chain and the −3 acetyl group is compensated, in part, by a new hydrogen bond between Ser[210] and the −3 side chain (Figure 7C). As Ser[210] is somewhat further from the −3 binding site (Figure 7D), the ligand relaxes to accommodate the new interaction. After the ligand fully relaxes (~175 ns), the hydrogen bond to the −3 acetyl group is almost completely lost. Additionally, the large aromatic residue, Trp[167], directly opposite Thr[276] in the cleft (Figure 7D), maintains contact with the substrate to some extent. Both of these interactions, with Ser[210] and Trp[167], allows the variant to bind $(GlcNAc)_6$ with slightly reduced affinity. As we will describe, the loss of the single hydrogen bond between the −3 carbonyl oxygen and the protein propagates to the dynamics along the binding cleft and greatly influences processive ability.

Similarly, the ligand-bound ChiA crystal structure depicts Arg[172] participating in a bifurcated hydrogen bond with the −3 pyranose and Glu[473] (30). The structure also illustrates Arg[172] forming a hydrogen bond with the −4 pyranose, along with residues Gly[171], Glu[208], Ser[210], and His[229]. On the basis of these structural observations, we hypothesized Arg[172] likely plays a role in substrate binding and that mutation to alanine would substantially reduce ligand interactions and affinity. However, MD simulation reveals that the hydrogen bond formed between Arg[172] and the GlcNAc ligand in the −3 binding site in wild-type ChiA is not persistent (Figure 7E). While mutation of Arg[172] to alanine completely abolishes any hydrogen bonds between this residue and the −3 pyranose, the intermittent nature of hydrogen bonding in wild-type indicates the hydrogen bond rarely exists and is not critical to ligand binding. Rather, Glu[473] appears to be responsible for the bulk of hydrogen bonding with the −3 pyranose, with hydrogen bonding unaffected by the R172A mutation (Figure 7F). However, we anticipate the presence of Trp[167] alone, residing directly next to both Arg[172] and Glu[473], is sufficient to maintain ligand affinity with the loss of hydrogen bonding from either residue. No significant difference in hydrogen bond patterns between subsite −4 and ChiA residues Gly[171], Glu[208], Ser[210], and His[229] was observed upon the R172A mutation.

The RMSF of the ligand is perhaps most closely related to the binding affinity; a ligand able to fluctuate to any significant degree in an enzyme binding site is unlikely to be strongly bound. In the case of the T276A variant, the $(GlcNAc)_6$ ligand fluctuates significantly more across the length of the cleft than ChiA-WT, while the ChiA-R172A ligand behaves roughly the same as ChiA-WT (Figure 6A). The results align with experimental measurements of binding affinity. The R172A mutation has little effect on the overall stability of the ligand, again indicating that the hydrogen bonds formed with the substrate in the −3 and −4 binding sites are not critical to binding. Rather, the remaining hydrogen bond with Glu[473] is sufficient to maintain stable binding. On the other hand, the broken hydrogen bond in subsite −3 resulting from the T276A mutation cannot be compensated by the surrounding protein, and the localized range of freedom translates across the length of the active site.

The RMSF of the protein catalytic center, residues Asp[313], Glu[315], Tyr[390], and Asp[391], also indicates that protein fluctuation correlates with binding affinity, wherein increased fluctuation corresponds to lower binding affinity. These catalytic residues are responsible for maintaining a suitable reactive

ligand conformation in the −1/+1 binding site (78,79). We observe that the fluctuation of the catalytic tetrad in ChiA-R172A is within error of ChiA-WT, but that ChiA-T276A fluctuates significantly more in this critical region of the active site (Figure 6B). Previously, we hypothesized that both RMSF of the ligand and the catalytic center is a molecular "hallmark" of processivity (71). This prior study focused on the delineation between processive and non-processive chitinases rather than variations as a result of mutagenesis. The results we present here confirm the observed relationship between active site dynamics and processive ability and extend its relevance to mutations of the same enzyme. The link between catalytic center flexibility and processivity is likely a result of the need, either evolutionarily or engineered, to associate and dissociate quickly from the substrate. Flexibility in the active site affords the enzyme with momentum to escape chemical attraction.

Related to the dynamics of the catalytic center, the conformation of the pyranose sugar in the −1 binding site illustrates the new dynamics imposed by the R172A and T276A mutations. The Cremer-Pople ring puckering amplitude of the −1 site pyranose ring was calculated over the 250-ns MD simulations for all three enzymes (Figure 6C) (74). Structural studies indicate that the ChiA ligand forms an approximate boat conformation along the catalytic itinerary of the substrate-assisted mechanism (78). Both ChiA-WT and ChiA-R172A maintain the structural conformation of the ring in the −1 binding site over the length of the simulation. However, ChiA-T276A allows the −1 pyranose to relax to the chair conformation after approximately 130 ns. The catalytic conformation is never recovered, indicating that the active site does not maintain as close an association with the substrate in the −1 binding site. This is particularly suggestive of the role T276A indirectly plays in catalysis. As previously mentioned, T276A primarily interacts with the substrate in the −2 and −3 binding subsites, yet clearly affects the dynamics of the entire binding site.

Chitosan degradation experiments suggest that Arg[172] is responsible in part for the recognition and positioning of the oligomer in the active site. In the case of ChiA-R172A, the variety in oligomeric reaction products produced by the variant implies the enzyme had no strong preferences for either acetylated or deacetylated units in subsites other than −1. In comparison, wild-type ChiA requires an acetylated moiety in subsites −1, −2, and −4. This result is particularly interesting, as Arg[172] appears to interact with as many as three different sugar moieties (−2, −3, and −4). Thus, despite having no role in processive activity, Arg[172] is central in the recognition and positioning of the substrate into the active site.

Similarly, chitosan degradation experiments reveal that the strong interacting ChiA-T276 that mainly binds with the −2 sugar does not appear to significantly affect the positioning of the substrate. Rather, the only prominent change in the chitosan degradation profile resulting from the T276A mutation is the more stringent requirement for an acetylated unit in the −3 binding site. This arises as a result of compensatory interactions made within the ChiA-T276A binding site that enables the ligand to remain bound. Naturally, one might think that deletion of the Thr[276] side chain, which forms a hydrogen bond with the −3 *N*-acetyl group would randomize the acceptance of acetylated or deacetylated groups in the mutant binding site; however, to maintain sufficient contact with the enzyme active site, a new hydrogen bond is formed between the −3 acetyl group and the nearby Ser[210] (Figure 7C and 7D). Until the relaxation of the entire ligand (following alleviation of ring distortion at ~130 ns), Ser[210] takes over ligand stabilization, allowing a modicum of remaining activity.

Finally, processive ability correlates with the rate and extent of chitin degradation. The enzymes with a higher initial degree of processivity are both faster and more efficient degraders of *β*-chitin (Figures 3 and 4). Drastic reduction in rate of hydrolysis and efficiency combined with reduction in processivity has previously been shown for aromatic residues in both ChiA and ChiB from *S. marcescens* (18,19). This result supports the notion that overall substrate turnover is improved by processivity, which results from the ability to maintain proximity with the substrate after each catalytic event.

From both simulation results and experimental evidence, we suggest that T276A is critical to formation of a stable, processive chitinase, while

R172A does not play a significant role in processive action. Prior studies have suggested that both hydrophobic stacking interactions and hydrogen bonding are important for a smooth processive cycle (22), and our results indicate that beyond that canonical carbohydrate-aromatic stacking interactions, polar residues can play a key role in this process. In particular, Thr^{276} in the ChiA active site is important to processive function. The fact that Arg^{172} does not participate in processive function indicates that replacement could be beneficial for enhanced processive action. Furthermore, our findings provide the first qualitative experimental characterization of the hypothesized relationship of binding affinity to GH processive action (10). The free energy of binding chito-oligosaccharides and allosamidin are indicative of processive ability. Perhaps the most interesting finding was that the inhibitor binding provided a more sensitive characterization of the relationship between binding and processivity. On the whole, our results provide new and valuable insight into the role polar residues along the length of a GH active site contributes to molecular interactions, substrate binding, and processivity in chitinases. More broadly, we suggest our results represent an important first step toward validating a hypothesized relationship that potentially describes the action of an entire class of GHs and greatly compliments our understanding of how GHs are able to depolymerize recalcitrant polysaccharides.

Reference List

1.   Gardner, K. H., and Blackwell, J. (1975) Refinement of the structure of β-chitin. *Biopolymers* **14**, 1581-1595
2.   Kim, J., Yun, S., and Ounaies, Z. (2006) Discovery of cellulose as a smart material. *Macromolecules* **39**, 4202-4206
3.   Tharanathan, R. N., and Kittur, F. S. (2003) Chitin-the undisputed biomolecule of great potential. *Crit. Rev. Food Sci. Nutr.* **43**, 61-87
4.   Lombard, V., Golaconda Ramulu, H., Drula, E., Coutinho, P. M., and Henrissat, B. (2014) The carbohydrate-active enzymes database (CAZy) in 2013. *Nucleic Acids Res.* **42**, D490-495
5.   Sinnott, M. L. (1990) Catalytic mechanisms of enzymatic glycosyl transfer. *Chem Rev* **90**, 1171-1202
6.   Davies, G., and Henrissat, B. (1995) Structures and mechanisms of glycosyl hydrolases. *Structure* **3**, 853-859
7.   Teeri, T. T. (1997) Crystalline cellulose degradation: New insight into the function of cellobiohydrolases. *Trends Biotechnol* **15**, 160-167
8.   von Ossowski, I., Ståhlberg, J., Koivula, A., Piens, K., Becker, D., Boer, H., Harle, R., Harris, M., Divne, C., Mahdi, S., Zhao, Y. X., Driguez, H., Claeyssens, M., Sinnott, M. L., and Teeri, T. T. (2003) Engineering the exo-loop of *Trichoderma reesei* cellobiohydrolase, Ce17A. A comparison with *Phanerochaete chrysosporium* Cel7D. *J. Mol. Biol.* **333**, 817-829
9.   Beckham, G. T., Ståhlberg, J., Knott, B. C., Himmel, M. E., Crowley, M. F., Sandgren, M., Sørlie, M., and Payne, C. M. (2014) Towards a molecular-level theory of carbohydrate processivity in glycoside hydrolases. *Curr. Opin. Biotechnol.* **27C**, 96-106
10.   Payne, C. M., Jiang, W., Shirts, M. R., Himmel, M. E., Crowley, M. F., and Beckham, G. T. (2013) Glycoside hydrolase processivity is directly related to oligosaccharide binding free energy. *J. Am. Chem. Soc.* **135**, 18831-18839
11.   Zolotnitsky, G., Cogan, U., Adir, N., Solomon, V., Shoham, G., and Shoham, Y. (2004) Mapping glycoside hydrolase substrate subsites by isothermal titration calorimetry. *Proc. Natl. Acad. Sci. U. S. A.* **101**, 11275-11280
12.   Vyas, N. K. (1991) Atomic features of protein-carbohydrate interactions. *Curr. Opin. Struct. Biol.* **1**, 732-740
13.   Rouvinen, J., Bergfors, T., Teeri, T., Knowles, J. K., and Jones, T. A. (1990) Three-dimensional structure of cellobiohydrolase II from *Trichoderma reesei. Science* **249**, 380-386
14.   Varrot, A., Frandsen, T. P., von Ossowski, I., Boyer, V., Cottaz, S., Driguez, H., Schulein, M., and Davies, G. J. (2003) Structural basis for ligand binding and processivity in cellobiohydrolase Cel6A from *Humicola insolens. Structure* **11**, 855-864
15.   Uchiyama, T., Katouno, F., Nikaidou, N., Nonaka, T., Sugiyama, J., and Watanabe, T. (2001) Roles of the exposed aromatic residues in crystalline chitin hydrolysis by chitinase A from *Serratia marcescens* 2170. *J. Biol. Chem.* **276**, 41343-41349
16.   Watanabe, T., Ariga, Y., Sato, U., Toratani, T., Hashimoto, M., Nikaidou, N., Kezuka, Y., Nonaka, T., and Sugiyama, J. (2003) Aromatic residues within the substrate-binding cleft of *Bacillus circulans* chitinase A1 are essential for hydrolysis of crystalline chitin. *Biochem. J.* **376**, 237-244

17. Zhou, W., Irwin, D. C., Escovar-Kousen, J., and Wilson, D. B. (2004) Kinetic studies of *Thermobifida fusca* Cel9A active site mutant enzymes. *Biochemistry* **43**, 9655-9663

18. Horn, S. J., Sikorski, P., Cederkvist, J. B., Vaaje-Kolstad, G., Sørlie, M., Synstad, B., Vriend, G., Vårum, K. M., and Eijsink, V. G. (2006) Costs and benefits of processivity in enzymatic degradation of recalcitrant polysaccharides. *Proc. Natl. Acad. Sci. USA* **103**, 18089-18094

19. Zakariassen, H., Aam, B. B., Horn, S. J., Vårum, K. M., Sørlie, M., and Eijsink, V. G. (2009) Aromatic residues in the catalytic center of chitinase A from *Serratia marcescens* affect processivity, enzyme activity, and biomass converting efficiency. *J. Biol. Chem.* **284**, 10610-10617

20. Proctor, M. R., Taylor, E. J., Nurizzo, D., Turkenburg, J. P., Lloyd, R. M., Vardakou, M., Davies, G. J., and Gilbert, H. J. (2005) Tailored catalysts for plant cell-wall degradation: redesigning the exo/endo preference of Cellvibrio japonicus arabinanase 43A. *Proc. Natl. Acad. Sci. USA* **102**, 2697-2702

21. Bu, L., Beckham, G. T., Shirts, M. R., Nimlos, M. R., Adney, W. S., Himmel, M. E., and Crowley, M. F. (2011) Probing carbohydrate product expulsion from a processive cellulase with multiple absolute binding free energy methods. *J. Biol. Chem.* **286**, 18161-18169

22. Meyer, J. E., and Schulz, G. E. (1997) Energy profile of maltooligosaccharide permeation through maltoporin as derived from the structure and from a statistical analysis of saccharide-protein interactions. *Protein Sci.* **6**, 1084-1091

23. Fuchs, R. L., McPherson, S. A., and Drahos, D. J. (1986) Cloning of a *Serratia marcescens* gene encoding chitinase. *Appl. Environ. Microbiol.* **51**, 504-509

24. Vaaje-Kolstad, G., Horn, S. J., Sørlie, M., and Eijsink, V. G. (2013) The chitinolytic machinery of *Serratia marcescens*--a model system for enzymatic degradation of recalcitrant polysaccharides. *FEBS J.* **280**, 3028-3049

25. Igarashi, K., Uchihashi, T., Uchiyama, T., Sugimoto, H., Wada, M., Suzuki, K., Sakuda, S., Ando, T., Watanabe, T., and Samejima, M. (2014) Two-way traffic of glycoside hydrolase family 18 processive chitinases on crystalline chitin. *Nat. Commun.* **5**, 3975

26. Monreal, J., and Reese, E. T. (1969) The chitinase of *Serratia marcescens*. *Can. J. Microbiol.* **15**, 689-696

27. Papanikolau, Y., Prag, G., Tavlas, G., Vorgias, C. E., Oppenheim, A. B., and Petratos, K. (2001) High resolution structural analyses of mutant chitinase A complexes with substrates provide new insight into the mechanism of catalysis. *Biochemistry* **40**, 11338-11343

28. Hult, E. L., Katouno, F., Uchiyama, T., Watanabe, T., and Sugiyama, J. (2005) Molecular directionality in crystalline β-chitin: hydrolysis by chitinases A and B from *Serratia marcescens* 2170. *Biochem. J.* **388**, 851-856

29. Horn, S. J., Sørbotten, A., Synstad, B., Sikorski, P., Sørlie, M., Vårum, K. M., and Eijsink, V. G. (2006) Endo/exo mechanism and processivity of family 18 chitinases produced by *Serratia marcescens*. *FEBS J.* **273**, 491-503

30. Norberg, A. L., Dybvik, A. I., Zakariassen, H., Mormann, M., Peter-Katalinic, J., Eijsink, V. G., and Sørlie, M. (2011) Substrate positioning in chitinase A, a processive chito-biohydrolase from *Serratia marcescens*. *FEBS Lett.* **585**, 2339-2344

31. Sakuda, S., Isogai, A., Matsumoto, S., and Suzuki, A. (1987) Search for microbial insect growth regulators. II. Allosamidin, a novel insect chitinase inhibitor. *J. Antibiot. (Tokyo)* **40**, 296-300

32.   Sakuda, S., Isogai, A., Matsumoto, S., Suzuki, A., and Koseki, K. (1986) The structure of allosamidin, a novel insect chitinase inhibitor, produced by *Streptomyces Sp. Tetrahedron Lett.* **27**, 2475-2478

33.   Brurberg, M. B., Eijsink, V. G., and Nes, I. F. (1994) Characterization of a chitinase gene (chiA) from *Serratia marcescens* BJL200 and one-step purification of the gene product. *FEMS Microbiol. Lett.* **124**, 399-404

34.   Brurberg, M. B., Nes, I. F., and Eijsink, V. G. (1996) Comparative studies of chitinases A and B from *Serratia marcescens. Microbiology* **142 (Pt 7)**, 1581-1589

35.   Norberg, A. L., Karlsen, V., Hoell, I. A., Bakke, I., Eijsink, V. G. H., and Sørlie, M. (2010) Determination of substrate binding energies in individual subsites of a family 18 chitinase. *FEBS Lett.* **584**, 4581-4585

36.   Sørbotten, A., Horn, S. J., Eijsink, V. G., and Vårum, K. M. (2005) Degradation of chitosans with chitinase B from *Serratia marcescens*. Production of chito-oligosaccharides and insight into enzyme processivity. *FEBS J.* **272**, 538-549

37.   Cederkvist, F. H., Parmer, M. P., Vårum, K. M., Eijsink, V. G. H., and Sørlie, M. (2008) Inhibition of a family 18 chitinase by chitooligosaccharides. *Carbohyd. Polym.* **74**, 41-49

38.   Bahrke, S., Einarsson, J. M., Gislason, J., Haebel, S., Letzel, M. C., Peter-Katalinic, J., and Peter, M. G. (2002) Sequence analysis of chitooligosaccharides by matrix-assisted laser desorption ionization postsource decay mass spectrometry. *Biomacromolecules* **3**, 696-704

39.   Hamre, A. G., Lorentzen, S. B., Väljamäe, P., and Sørlie, M. (2014) Enzyme processivity changes with the extent of recalcitrant polysaccharide degradation. *FEBS Lett.* **588**, 4620-4624

40.   Wiseman, T., Williston, S., Brandts, J. F., and Lin, L. N. (1989) Rapid measurement of binding constants and heats of binding using a new titration calorimeter. *Anal. Biochem.* **179**, 131-137

41.   Krokeide, I. M., Synstad, B., Gåseidnes, S., Horn, S. J., Eijsink, V. G., and Sørlie, M. (2007) Natural substrate assay for chitinases using high-performance liquid chromatography: a comparison with existing assays. *Anal. Biochem.* **363**, 128-134

42.   Zakariassen, H., Hansen, M. C., Jøranli, M., Eijsink, V. G., and Sørlie, M. (2011) Mutational effects on transglycosylating activity of family 18 chitinases and construction of a hypertransglycosylating mutant. *Biochemistry* **50**, 5693-5703

43.   van Aalten, D. M., Komander, D., Synstad, B., Gåseidnes, S., Peter, M. G., and Eijsink, V. G. (2001) Structural insights into the catalytic mechanism of a family 18 exo-chitinase. *Proc. Natl. Acad. Sci. USA* **98**, 8979-8984

44.   Anandakrishnan, R., Aguilar, B., and Onufriev, A. V. (2012) H++ 3.0: automating pK prediction and the preparation of biomolecular structures for atomistic molecular modeling and simulations. *Nucleic Acids Res.* **40**, W537-541

45.   Myers, J., Grothaus, G., Narayanan, S., and Onufriev, A. (2006) A simple clustering algorithm can be accurate enough for use in calculations of pKs in macromolecules. *Proteins* **63**, 928-938

46.   Gordon, J. C., Myers, J. B., Folta, T., Shoja, V., Heath, L. S., and Onufriev, A. (2005) H++: a server for estimating pKas and adding missing hydrogens to macromolecules. *Nucleic Acids Res.* **33**, W368-371

47.   Brooks, B. R., Brooks, C. L., 3rd, Mackerell, A. D., Jr., Nilsson, L., Petrella, R. J., Roux, B., Won, Y., Archontis, G., Bartels, C., Boresch, S., Caflisch, A., Caves, L., Cui, Q., Dinner, A. R., Feig, M., Fischer, S., Gao, J., Hodoscek, M., Im, W., Kuczera, K.,

Lazaridis, T., Ma, J., Ovchinnikov, V., Paci, E., Pastor, R. W., Post, C. B., Pu, J. Z., Schaefer, M., Tidor, B., Venable, R. M., Woodcock, H. L., Wu, X., Yang, W., York, D. M., and Karplus, M. (2009) CHARMM: the biomolecular simulation program. *J. Comput. Chem.* **30**, 1545-1614

48. Mackerell, A. D., Feig, M., and Brooks, C. L. (2004) Extending the treatment of backbone energetics in protein force fields: Limitations of gas-phase quantum mechanics in reproducing protein conformational distributions in molecular dynamics simulations. *J. Comput. Chem.* **25**, 1400-1415

49. MacKerell, A. D., Bashford, D., Bellott, M., Dunbrack, R. L., Evanseck, J. D., Field, M. J., Fischer, S., Gao, J., Guo, H., Ha, S., Joseph-McCarthy, D., Kuchnir, L., Kuczera, K., Lau, F. T., Mattos, C., Michnick, S., Ngo, T., Nguyen, D. T., Prodhom, B., Reiher, W. E., Roux, B., Schlenkrich, M., Smith, J. C., Stote, R., Straub, J., Watanabe, M., Wiorkiewicz-Kuczera, J., Yin, D., and Karplus, M. (1998) All-atom empirical potential for molecular modeling and dynamics studies of proteins. *The journal of physical chemistry. B* **102**, 3586-3616

50. Durell, S. R., Brooks, B. R., and Bennaim, A. (1994) Solvent-induced forces between 2 hydrophilic groups. *J. Phys. Chem.* **98**, 2198-2202

51. Jørgensen, W. L., Chandrasekhar, J., Madura, J. D., Impey, R. W., and Klein, M. L. (1983) Comparison of simple potential functions for simulating liquid water. *J Chem Phys* **79**, 926-935

52. Hoover, W. G. (1985) Canonical dynamics: Equilibrium phase-space distributions. *Phys. Rev. A* **31**, 1695-1697

53. Nose, S., and Klein, M. L. (1983) Constant pressure molecular-dynamics for molecular-systems. *Mol. Phys.* **50**, 1055-1076

54. Phillips, J. C., Braun, R., Wang, W., Gumbart, J., Tajkhorshid, E., Villa, E., Chipot, C., Skeel, R. D., Kalé, L., and Schulten, K. (2005) Scalable molecular dynamics with NAMD. *J. Comput. Chem.* **26**, 1781-1802

55. Essmann, U., Perera, L., Berkowitz, M. L., Darden, T., Lee, H., and Pedersen, L. G. (1995) A smooth particle mesh ewald method. *The Journal of chemical physics* **103**, 8577-8593

56. Ryckaert, J. P., Ciccotti, G., and Berendsen, H. J. C. (1977) Numerical-integration of cartesian equations of motion of a system with constraints - molecular-dynamics of N-alkanes. *J. Comput. Phys.* **23**, 327-341

57. Humphrey, W., Dalke, A., and Schulten, K. (1996) VMD: visual molecular dynamics. *J. Mol. Graph.* **14**, 33-38, 27-38

58. Davies, G. J., Wilson, K. S., and Henrissat, B. (1997) Nomenclature for sugar-binding subsites in glycosyl hydrolases. *Biochem. J.* **321 (Pt 2)**, 557-559

59. Hackman, R. H. (1954) Studies on chitin. I. Enzymic degradation of chitin and chitin esters. *Aust. J. Biol. Sci.* **7**, 168-178

60. Sannan, T., Kurita, K., and Iwakura, Y. (1976) Studies on chitin, 2. Effect of deacetylation on solubility. *Macromol. Chem.* **177**, 3589-3600

61. Vårum, K. M., Anthonsen, M. W., Grasdalen, H., and Smidsrød, O. (1991) 13C-n.m.r. studies of the acetylation sequences in partially N-deacetylated chitins (chitosans). *Carbohydr. Res.* **217**, 19-27

62. Vårum, K. M., Anthonsen, M. W., Grasdalen, H., and Smidsrød, O. (1991) Determination of the degree of N-acetylation and the distribution of N-acetyl groups in partially N-

deacetylated chitins (chitosans) by high-field n.m.r. spectroscopy. *Carbohydr. Res.* **211**, 17-23

63. Synstad, B., Gåseidnes, S., Van Aalten, D. M., Vriend, G., Nielsen, J. E., and Eijsink, V. G. (2004) Mutational and computational analysis of the role of conserved residues in the active site of a family 18 chitinase. *Eur. J. Biochem.* **271**, 253-262

64. Terwisscha van Scheltinga, A. C., Armand, S., Kalk, K. H., Isogai, A., Henrissat, B., and Dijkstra, B. W. (1995) Stereochemistry of chitin hydrolysis by a plant chitinase/lysozyme and X-ray structure of a complex with allosamidin: evidence for substrate assisted catalysis. *Biochemistry* **34**, 15619-15623

65. Tews, I., Terwisscha van Scheltinga, A. C., Perrakis, A., Wilson, K. S., and Dijkstra, B. W. (1997) Substrate-assisted catalysis unifies two families of chitinolytic enzymes. *J. Am. Chem. Soc.* **119**, 7954-7959

66. Horn, S. J., Sørlie, M., Vårum, K. M., Väljamäe, P., and Eijsink, V. G. (2012) Measuring processivity. *Methods Enzymol.* **510**, 69-95

67. Kurasin, M., and Väljamäe, P. (2011) Processivity of cellobiohydrolases is limited by the substrate. *J. Biol. Chem.* **286**, 169-177

68. Igarashi, K., Uchihashi, T., Koivula, A., Wada, M., Kimura, S., Okamoto, T., Penttila, M., Ando, T., and Samejima, M. (2011) Traffic jams reduce hydrolytic efficiency of cellulase on cellulose surface. *Science* **333**, 1279-1282

69. Kostylev, M., Alahuhta, M., Chen, M., Brunecky, R., Himmel, M. E., Lunin, V. V., Brady, J., and Wilson, D. B. (2014) Cel48A from Thermobifida fusca: structure and site directed mutagenesis of key residues. *Biotechnol. Bioeng.* **111**, 664-673

70. Baban, J., Fjeld, S., Sakuda, S., Eijsink, V. G. H., and Sørlie, M. (2010) The roles of three *Serratia marcescens* chitinases in chitin conversion are reflected in different thermodynamic signatures of allosamidin binding. *The journal of physical chemistry. B* **114**, 6144-6149

71. Payne, C. M., Baban, J., Horn, S. J., Backe, P. H., Arvai, A. S., Dalhus, B., Bjørås, M., Eijsink, V. G., Sørlie, M., Beckham, G. T., and Vaaje-Kolstad, G. (2012) Hallmarks of processivity in glycoside hydrolases from crystallographic and computational studies of the *Serratia marcescens* chitinases. *J. Biol. Chem.* **287**, 36322-36330

72. Blake, C. C., Johnson, L. N., Mair, G. A., North, A. C., Phillips, D. C., and Sarma, V. R. (1967) Crystallographic studies of the activity of hen egg-white lysozyme. *Proc. R. Soc. Lond. B. Biol. Sci.* **167**, 378-388

73. Phillips, D. C. (1966) The three-dimensional structure of an enzyme molecule. *Sci. Am.* **215**, 78-90

74. Cremer, D., and Pople, J. A. (1975) General definition of ring puckering coordinates. *J. Am. Chem. Soc.* **97**, 1354-1358

75. Hill, A. D., and Reilly, P. J. (2007) Puckering coordinates of monocyclic rings by triangular decomposition. *J. Chem. Inf. Model.* **47**, 1031-1035

76. Colussi, F., Sørensen, T. H., Alasepp, K., Kari, J., Cruys-Bagger, N., Windahl, M. S., Olsen, J. P., Borch, K., and Westh, P. (2015) Probing substrate interactions in the active tunnel of a catalytically deficient cellobiohydrolase (cel7). *J. Biol. Chem.* **290**, 2444-2454

77. Cooper, A., Johnson, C. M., Lakey, J. H., and Nöllmann, M. (2001) Heat does not come in different colours: entropy-enthalpy compensation, free energy windows, quantum confinement, pressure perturbation calorimetry, solvation and the multiple causes of heat capacity effects in biomolecular interactions. *Biophys. Chem.* **93**, 215-230

78. Brameld, K. A., and Goddard, W. A. (1998) Substrate distortion to a boat conformation at subsite −1 is critical in the mechanism of family 18 chitinases. *J. Am. Chem. Soc.* **120**, 3571-3580

79. Aronson, N. N., Halloran, B. A., Alexeyev, M. F., Zhou, X. E., Wang, Y., Meehan, E. J., and Chen, L. (2006) Mutation of a conserved tryptophan in the chitin-binding cleft of *Serratia marcescens* chitinase A enhances transglycosylation. *Biosci. Biotech. Biochem.* **70**, 243-251

80. Towns, J., Cockerill, T., Dahan, M., Foster, I., Gaither, K., Grimshaw, A., Hazlewood, V., Lathrop, S., Lifka, D., Peterson, G. D., Roskies, R., Scott, J. R., and Wilkins-Diehr, N. (2014) XSEDE: Accelerating scientific discovery. *Comput. Sci. Eng.* **16**, 62-74

81. Dybvik, A. I., Norberg, A. L., Schute, V., Soltwisch, J., Peter-Katalinic, J., Vårum, K. M., Eijsink, V. G., Dreisewerd, K., Mormann, M., and Sørlie, M. (2011) Analysis of noncovalent chitinase-chito-oligosaccharide complexes by infrared-matrix assisted laser desorption ionization and nanoelectrospray ionization mass spectrometry. *Anal. Chem.* **83**, 4030-4036

ACKNOWLEDGEMENTS

FOOTNOTES

[1]A. G. Hamre and S. Jana contributed equally to this work.

[2]To whom correspondence should be addressed: E-mail address: morten.sorlie@nmbu.no and christy.payne@uky.edu Tel.: +47-67232562 and Fax: +47-64965901 (MS); Tel.: + 859-257-2902 and Fax: + 859-323-1929 (CMP).

[3] The abbreviations used are: ΔG_r°, reaction free energy change; ΔH°_r, the reaction enthalpy change; ΔS_r°, reaction entropy change; **A**, N-acetyl-glucosamine; ABNR, adopted basis Newton-Raphson; AMAC, 2-aminoacridone; ChiA, Chitinase A; CHOS, chito-oligosaccharides; **D**, N-glucosamine; DHB, 2,5-dihydroxybenzoic acid; DP, degree of polymerization; F_A, fraction of N-acetylated units; GH, glycoside hydrolase; GlcNAc, N-acetyl-glucosamine; GlcN, N-glucosamine; ITC, isotherm titration calorimetry; K_a, the equilibrium binding association constant; K_d, the equilibrium binding dissociation constant; MD, molecular dynamics; n, the stoichiometry; P^{app}, apparent processivity; RMSF, the root mean square fluctuation; SD, steepest descent; TB, terrific broth

FIGURE LEGENDS

Figure 1. Crystal structures of the active site of ChiA in the presence of (GlcNAc)$_6$ (A, colored grey) and allosamidin (B, colored yellow). Highlighted in green are the two residues investigated in this study (Thr^{276} and Arg^{172}). Other important substrate binding residues (Trp^{167}, Glu^{473}, Asp^{313} and Glu^{315}) are highlighted in orange while product binding residues (Trp^{275}, Tyr^{390} and Asp^{391}) are shown in cyan.

Figure 2. Comparison of initial [(GlcNAc)$_2$/(GlcNAc)] ratios for ChiA wt (■), ChiA-R172A (●) and ChiA-T276A (▲). Hydrolysis was undertaken with 2.5 µM enzyme, pH 6.1 sodium acetate buffer at t = 37 °C with 2.0 mg/ml chitin. Error bars represent standard deviation of duplicate experiments. WT control experiments were conducted at the same time as the variant experiments and were in agreement with previously published values, which have been provided here for comparison (39).

Figure 3. Progress curves for the formation of (GlcNAc)$_2$ (squares) and GlcNAc (circles) after hydrolysis of b-chitin by ChiA wt (black), ChiA-R172A (red), and ChiA-T276A (green). (GlcNAc)$_2$ and GlcNAc were the only products detected. A clear correlation between initial rates and P^{app} is observed. WT control experiments were conducted at the same time as the variant experiments and were in agreement with previously published values, which have been provided here for comparison (39).

Figure 4. Relationship of the [(GlcNAc)$_2$/(GlcNAc)] ratio for ChiA wt (■), ChiA-R172A (●) and ChiA-T276A (▲) with extent of degradation. Hydrolysis was undertaken with 2.5 µM enzyme, pH 6.1 sodium acetate buffer at t = 37 °C with 2.0 mg/ml chitin. Error bars represent standard deviation of duplicate experiments. WT control experiments were conducted at the same time as the variant experiments and were in agreement with previously published values, which have been provided here for comparison (39).

Figure 5. Top: Thermograms (upper panels) and binding isotherms with theoretical fits (lower panels) obtained for the binding of allosamidin to ChiA-WT (left), ChiA-T276A (middle), and ChiA-R172A (right) at t = 30 °C in 20 mM potassium phosphate at pH 6.0.
Bottom: Thermograms (upper panels) and binding isotherms with theoretical fits (lower panels) obtained for the binding of (GlcNAc)$_6$ to Chi-WT (left), ChiA-T276A (middle), and ChiA-R172A (right) at t = 30 °C in 20 mM potassium phosphate at pH 6.0.

Figure 6. Dynamics of the ChiA-WT, ChiA-R172A, and ChiA-T276A active sites as determined from 250-ns MD simulations. (A) Root mean square fluctuation (RMSF) of the chito-oligosaccharide (GlcNAc)$_6$ given on a per-binding-site basis. (B) RMSF of the four residues implicated in catalysis, either directly or indirectly: Asp^{313}, Glu^{315}, Tyr^{390}, and Asp^{391}. In both panels (A) and (B) uncertainty of the RMSF value was obtained through block averaging (2.5 ns blocks). (C) Cremer-Pople ring pucker amplitude of the -1 site pyranose sugar ring over the entire 250-ns simulation. The boat conformation is represented by 0.73 Å, and chair conformation is represented by 0.57 Å (75)

Figure 7. Hydrogen bonds formed between ChiA residues and ligand subsites over 250-ns MD simulations. (A) Number of hydrogen bonds (hbonds) formed between wild-type ChiA Thr^{276} and ChiA-T276A Ala^{276} with the -3 subsite. (B) Number of hydrogen bonds formed between wild-type ChiA Thr^{276} and ChiA-T276A Ala^{276} with the −2 subsite. (C) Number of hydrogen bonds formed between wild-type ChiA Ser^{210} and ChiA-T276A Ser^{210} with the -3 subsite. (D) 100-ns snapshots from wild-type ChiA and ChiA-T276A MD simulations illustrating the loss of the wild-type Thr^{276}/-3 acetyl group hydrogen bond and formation of the Ser^{210}/-3 acetyl group hydrogen bond upon mutation to alanine. The ChiA protein is shown in cartoon. The chito-oligomer and highlighted residues are shown in cyan and red stick. Trp^{167} is highlighted in yellow stick. Distances are labeled in units of Å and indicated by dashed lines. (E) Number of hydrogen bonds formed between wild-type ChiA Arg^{172} and ChiA-R172A Ala^{172} with subsites -3 and −4. (F) Number of hydrogen bonds formed between wild-type ChiA and ChiA-R172A Glu^{473} and the -3

subsite. In this final panel, the data sets are shown as translucent overlays to indicate the abundance of hydrogen bonding regardless of mutation.

Table 1. Primers used for site-directed mutagenesis

Mutant	DNA template	Primer	Sequence
ChiA-R172A	ChiA-WT	Forward	5'- GGGGCGTTTACGGGGCCAATTTCACCGTCG-3'
		Reverse	5'- CGACGGTGAATTGGCCCCTAAACGCCCC-3'
ChiA-T276A	ChiA-WT	Forward	5'- TCGGCGGCTGGGCGCTGTCCGAC-3'
		Reverse	5'- GTCGGACAGCGCCCAGCCGCCGA-3'
ChiA-E315Q-R172A	ChiA-E315Q[a]	Forward	5'- GGGGCGTTTACGGGGCCAATTTCACCGTCG-3'
		Reverse	5'- CGACGGTGAATTGGCCCCTAAACGCCCC-3'
ChiA-E315Q-T276A	ChiA-E315Q[a]	Forward	5'- TCGGCGGCTGGGCGCTGTCCGAC-3'
		Reverse	5'- GTCGGACAGCGCCCAGCCGCCGA-3'

[a] (81)

Table 2. Kinetic Constants of ChiA-WT, ChiA-T276A, and ChiA-R172A for the hydrolysis of $(GlcNAc)_4$ in 20 mM Sodium Acetate, pH 6.1, and 0.1 mg/mL BSA at 37 °C.

Enzyme	k_{cat} (s^{-1})	K_m (µM)	k_{cat}/K_m (µM^{-1} s^{-1})
ChiA-WT[a]	33 ± 1	9 ± 1	4
ChiA-T276A	12 ± 2	7 ± 1	2
ChiA-R172A	39 ± 4	88 ± 12	0.4

[a] (41)

Table 3. Sequence determination of CHOS of DP = 5 obtained after hydrolysis of chitosan (F_A = 0.65) with ChiA-WT, ChiA-T267A, ChiA-R172A to a maximum degree of scission.

m/z	CHOS	Sequence WABC [a]	T276A	R172A
1124.252		-	-	DDADA-▲
1166.265	D2A3	DADAA-▲	-	DDAAA-▲
				DAADA-▲
				DADAA-▲
				ADADA-▲
				ADDAA-▲
1208.269	D1A4	AADAA-▲	DAAAA-▲	AAADA-▲
			AAADA-▲	ADAAA-▲

▲ represents the reducing end tag.
[a] (30)

Table 4. Thermodynamic Parameters for $(GlcNAc)_6$ and allosamidin binding to ChiA-WT, ChiA-T276A, ChiA-R172A from *Serratia marcescens* at $t = 30$ °C, pH = 6.0.

Enzyme	$K_d{}^a$	$\Delta G_r{}^{\circ b}$	$\Delta H_r{}^{\circ b}$	$-T\Delta S_r{}^{\circ b}$
		$(GlcNAc)_6$		
ChiA-WT[c]	0.56 ± 0.03	−8.7 ± 0.1	−4.5 ± 0.2	−4.2 ± 0.2
ChiA-T276A[c]	1.2 ± 0.2	−8.2 ± 0.1	−1.9 ± 0.2	−6.3 ± 0.2
ChiA-R172A[c]	0.61 ± 0.02	−8.6 ± 0.1	−4.8 ± 0.2	−3.8 ± 0.2
		Allosamidin		
ChiA-WT[d]	0.027 ± 0.002	−10.5 ± 0.1	−7.5 ± 0.3	−2.8 ± 0.3
ChiA-T276A	1.0 ± 0.1	−8.3 ± 0.1	−3.7 ± 0.2	−4.6 ± 0.2
ChiA-R172A	0.067 ± 0.008	−9.9 ± 0.1	−7.1 ± 0.1	−2.8 ± 0.1

[a] μM, [b] kcal/mol, [c] the catalytic acid Glu^{315} have been exchanged to Gln, [d] (70)

Figure 1

Figure 2

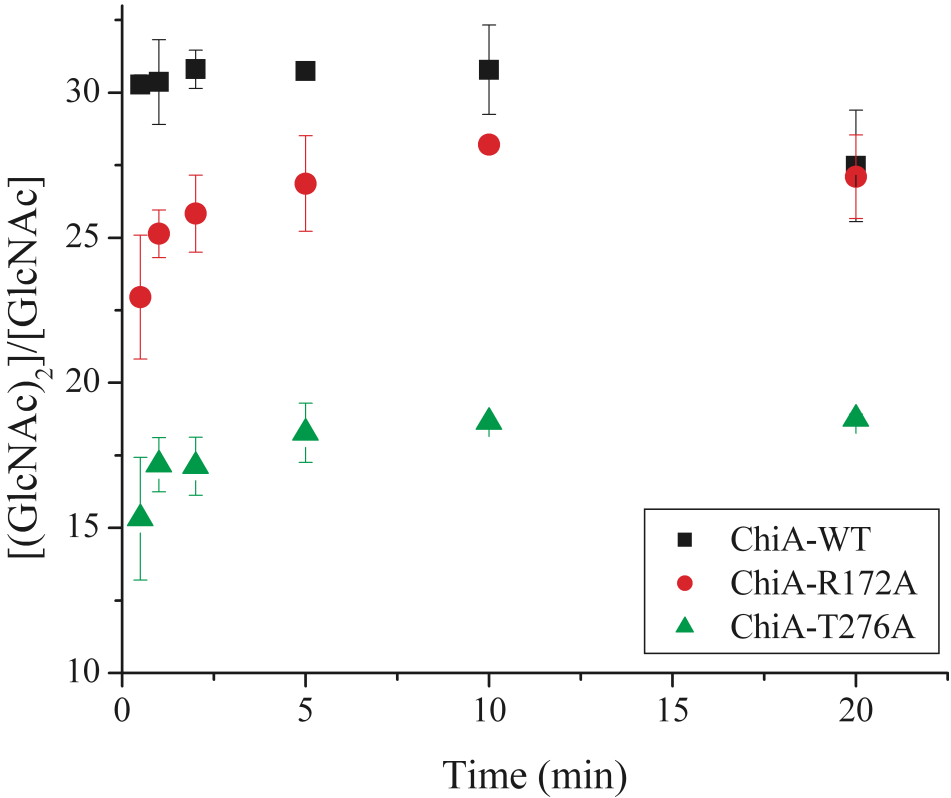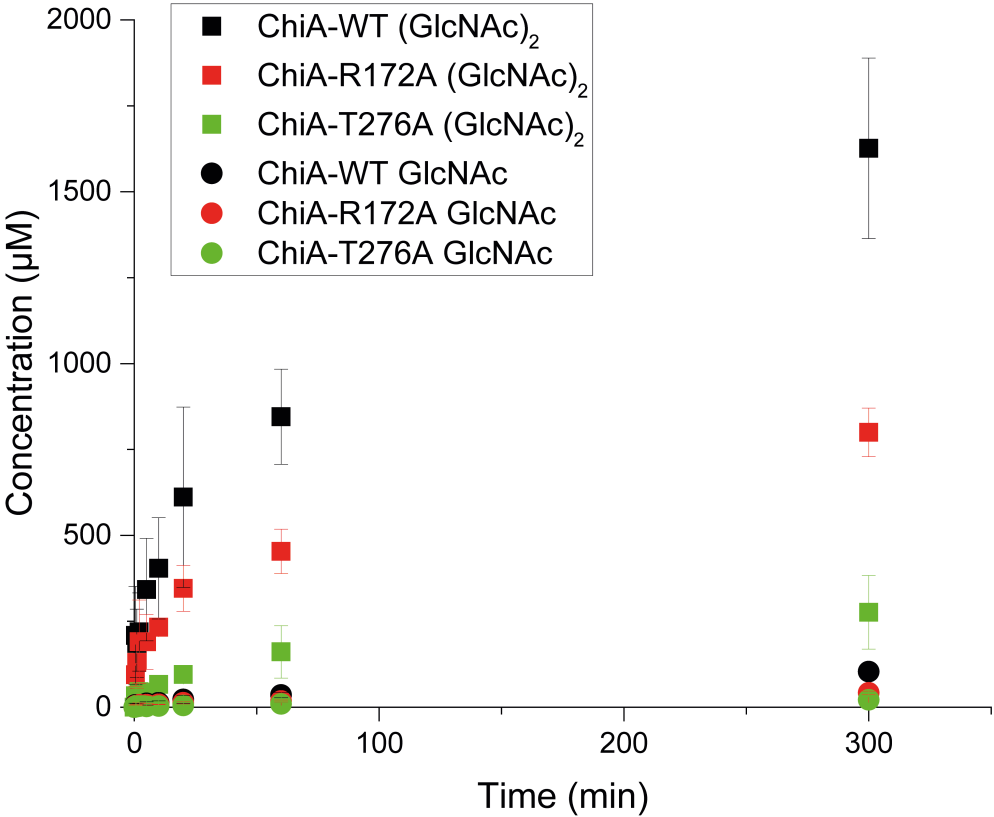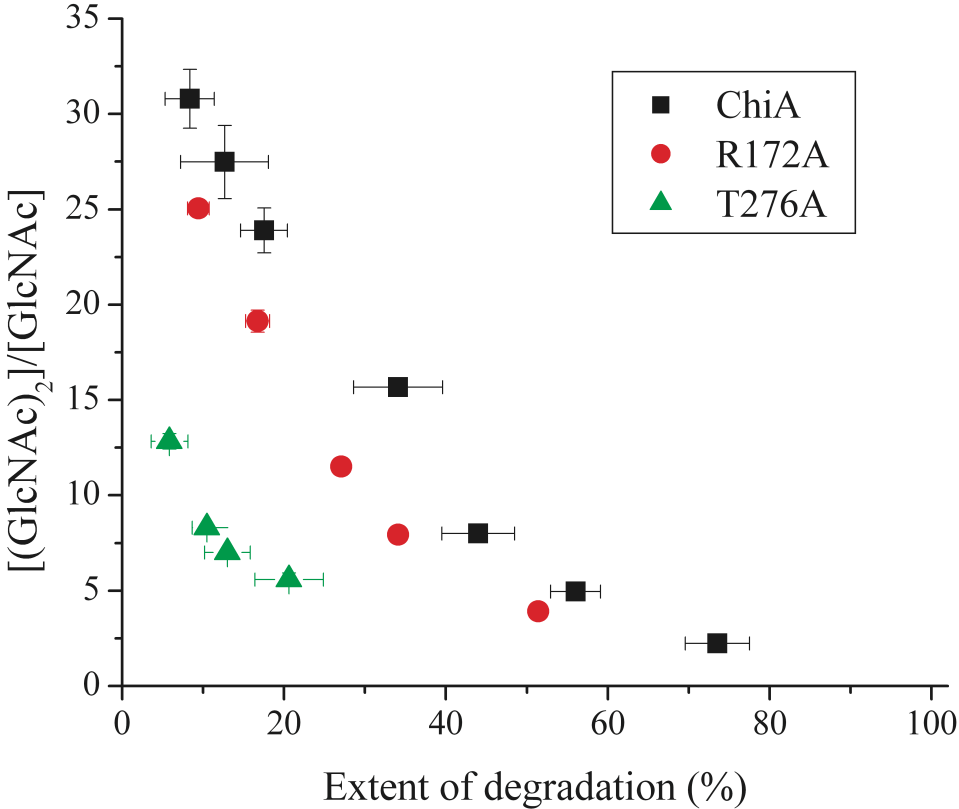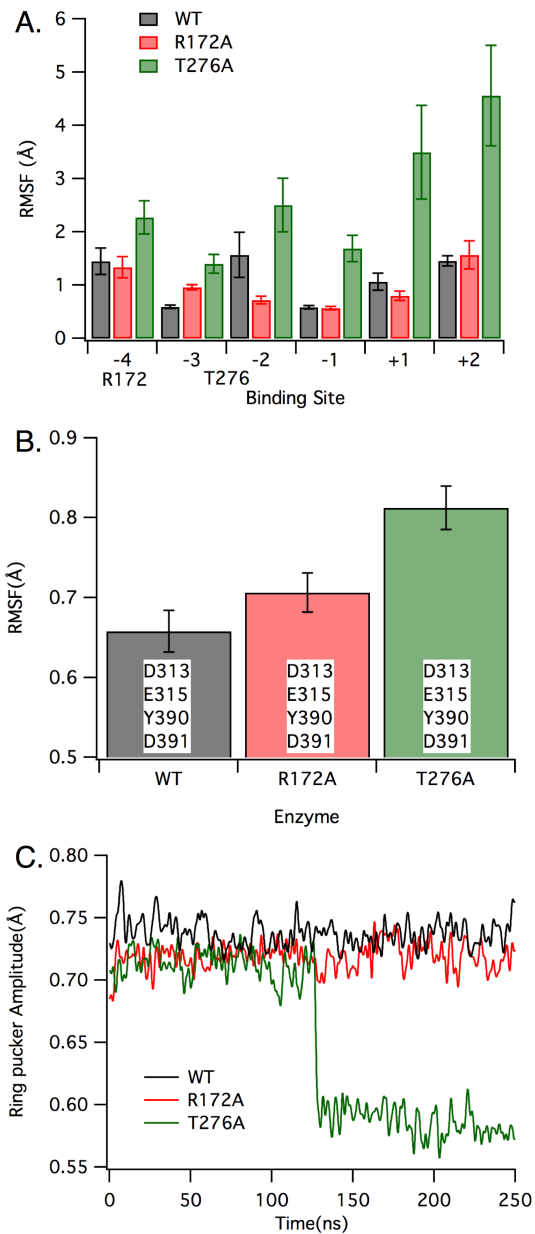The figure plots [(GlcNAc)₂]/[GlcNAc] versus Time (min) for ChiA-WT, ChiA-R172A, and ChiA-T276A.
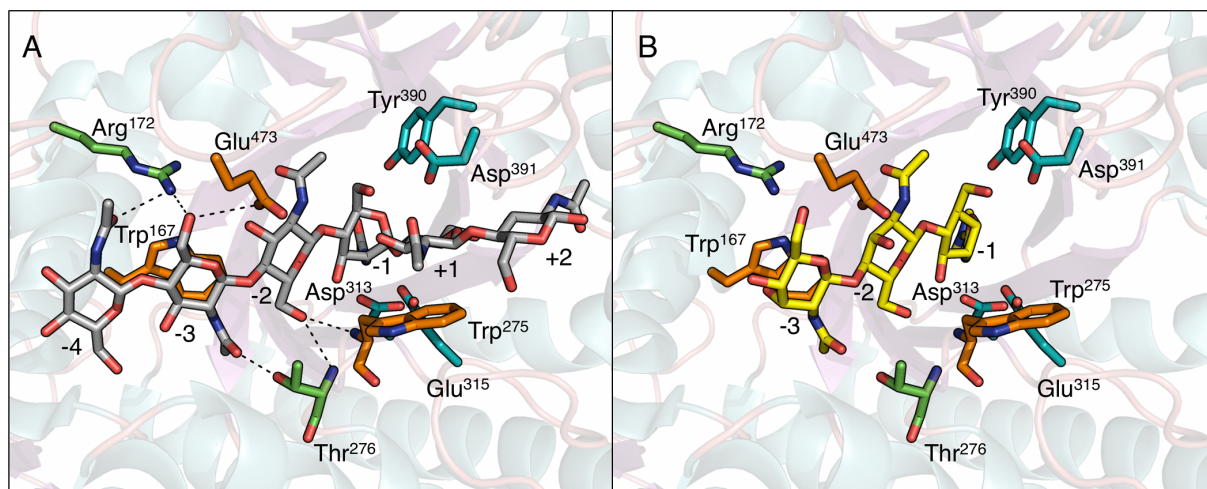
Figure 3

Figure 4

Figure 5

Figure 6

Figure 7